Biosystems Engineering 237 (2024) 71–82

Contents lists available at ScienceDirect

Biosystems Engineering

journal homepage: www.elsevier.com/locate/issn/15375110

Research Paper

Digital Twins analysis as a tool to find new descriptors for grapevine bunch morphology categorisation and grey mould infection risk evaluation

Alessandro Zanchin [a,*], Marco Sozzi [a], Domenico Giora [a], Mahshid Kalantari [b], Nicola Belfiore [c], Josef Terleth [d], Diego Tomasi [e], Francesco Marinello [a]

[a] Department of Land Environment Agriculture and Forestry, University of Padova, 35020, Legnaro, Italy
[b] Department of Agronomy, Food, Natural Resources, Animals, and Environment, University of Padova, 35020, Legnaro, Italy
[c] Research Centre for Viticulture and Enology, Council for Agricultural Research and Economics (CREA-VE), 31015, Conegliano, Italy
[d] Laimburg Research Centre, Laimburg, 39051, Italy
[e] Consorzio di Tutela del Conegliano Valdobbiadene Prosecco DOCG, 31053, Pieve di Soligo, Italy

ARTICLE INFO

Keywords:
Photogrammetry
Bunch morphology
Bunch compactness
Grey mould

ABSTRACT

Botrytis cinerea is one of the most destructive diseases for *Vitis vinifera*, and grape bunch morphology plays a crucial role in grey mould infection. However, the common visual evaluation technique for assessing bunch compactness suffers from a lack of sensitivity and objectivity. This study proposes a standardised digital twin shape analysis to evaluate the morphology of grape bunches. Seventeen Pinot Gris and six Pinot Noir clones were considered. The grey mould severity was evaluated in the field. Fully ripened bunches (138) were gathered and then photographed at different angles. Digital twin reconstruction was carried out using the photogrammetry technique. Several measures and indices were extracted from each digital twin. Principal component analysis and multiple linear regression models were applied to identify the descriptors most related to grey mould symptoms. The results revealed that the most significant factors include the berries density, the estimated empty volume, and the bunch width. These results show that digital twins are a suitable tool for estimating grey mould infection risks. Two linear models, divided into 2D and 3D descriptor models, were proposed. The R-squared value and the root mean square error were compared between the models. For Pinot Gris, from the 2D to the 3D models, the R-squared value rose from 0.656 to 0.838, while the error decreased from 1.713 to 1.175. In Pinot Noir, the 2D model did not provide sufficient robustness, while the 3D model had an R-squared value of 0.936 and an error of 0.290.

1. Introduction

Classifying *Vitis vinifera* varieties requires the observation and evaluation of many plant features. Bunch morphology is critical in classifying and describing *Vitis vinifera* varieties and different clones within the same variety. Bunch length, bunch width, peduncle length, density, bunch shape, number of wings, and bunch compactness are the primary descriptors proposed by the Organisation Internationale de la Vigne et du Vin (OIV). Additionally, the bunch's shape and compactness notably influence juice quality, pest infestation, and pathogen infection (Blank et al., 2019). In particular, the relationship between bunch compactness and grey mould (*Botrytis cinerea*) has been deeply investigated (Hed et al., 2009; Kocsis et al., 2018). Grey mould is one of the most destructive fungal diseases affecting many fruit crops, especially grapevine. *Botrytis cinerea* is the necrotrophic organism responsible for grey mould disease. The infection can occur from the flowering to the ripening stages of flowers and fruits (Ky et al., 2012).

Grey mould can ruin grape juice and, consequently, can undermine wine quality. According to Stummer et al. (2003), Chardonnay grapes affected by grey mould produced wines with a mouldy aroma and a lower value of total soluble solids as compared to test bunches. In the case of red wine, chemical analysis has shown an oxidation change in wine with a lower value of overall anthocyanins, a higher volatile acidity, changes in colour and flavour, and crucial difficulties for wine ageing (Ky et al., 2012). Furthermore, the protein produced by *Botrytis cinerea* can adversely affect the foam stability of sparkling wine, as stated by Marchal et al. (2020).

Botrytis cinerea is an enphytotic pathogen that occurs virtually every season in wet and cool continental regions (Molitor et al., 2016). Since

* Corresponding author.
E-mail address: alessandro.zanchin@phd.unipd.it (A. Zanchin).

https://doi.org/10.1016/j.biosystemseng.2023.10.019
Received 17 March 2023; Received in revised form 27 October 2023; Accepted 31 October 2023
Available online 14 December 2023

Nomenclature

OIV	Organisation Internationale de la Vigne et du Vin
DT	Digital Twin
MLR	Multiple Linear Regression Model
R^2	R-squared value
RMSE	Root Mean Square Error
TH	Townsend-Heuberger index (disease severity)
Cl	Optimal number of classes
N	Number of samples
V	Infection class
PG	Pinot Gris
PN	Pinot Noir
C	Cylindric shape
F	Funnel shape
PCA	Principal Component Analysis
AIC	Akaike Information Criterion
2D	Two-dimensional
3D	Three-dimensional
H	Horizontal section
V	Vertical section
x, z	Two orthogonal vertical sections
Dim1	First PCA dimension
Dim2	Second PCA dimension

climate plays a crucial role in grey mould severity, the microclimate throughout the vine canopy must be considered to prevent grey mould. Dense vegetation promotes humidity inside the plant canopy and wet microclimate conditions encourage grey mould to spread among grape clusters (Bem et al., 2015). Basal leaf removal is an affordable technique to increase airflow exchange, allowing sunlight to reach the grape bunches and shaded organs within the vine canopies (Würz et al., 2020). "Early defoliation" is the term for leaf removal that occurs from the preflowering to flowering stages. Early defoliation has been found to induce carbon deprivation in flowers, causing an energy shortage for fruit set (VanderWeide et al., 2021; Lebon et al., 2004) and reducing bunch compactness (Poni et al., 2006; Tardaguila et al., 2012).

Fungicide spraying plays a key role in preventing *Botrytis cinerea* infections. However, fungicides can have many secondary and adverse effects, such as promoting the selection of resistant fungal strains (Leroux & Tisseyre, 2019). In addition, the environmental policies of different countries state that pesticide application must be used as a last resort in pest management decision-making (Parliament, 2009).

Moreover, for decades, genetic selection has been attempted to identify clones among the most widely cultivated varieties that have traits of grey mould resistance (Artem et al., 2014).

Currently, grape bunch morphology description follows the OIV technical standard (OIV, 2009). In particular, descriptor 204 provides a guideline for classifying bunches based on a visual evaluation. However, the OIV technical standard proposes a visual assessment that requires a skilled evaluator and is time-consuming without taking into account specific bunch traits (Rist et al., 2018). Several authors have stated the need for an objective method for bunch compactness assessment based on bunch morphology to avoid human errors (Gatti et al., 2012; Palliotti et al., 2011; Tello & Ibáñez 2014, 2018). For this purpose, sensors and morphology analysis techniques have been explored. For example, Tello and Ibáñez (2014) proposed alternative measures and indices based on standard OIV descriptors, while other researchers have exploited image analysis to estimate several OIV descriptors and bunch compactness (Chen et al., 2018; Cubero et al., 2015; Lopes & Cadima, 2021; Underhill et al., 2020). Palacios et al. (2019) proposed an innovative methodology to assess bunch compactness directly in the field, exploiting artificial intelligence applied to 2D image analysis.

Other researchers have conducted digital model analyses to increase the number of features available for compactness assessment (Xin et al., 2020). Such analyses are based on the spatial distribution of the point cloud generated by digital model reconstructions of grape bunches. Each point returns the actual bunch shape and morphology (Herrero-Huerta et al., 2022). This type of analysis is a proven technique for predicting bunch compactness that is more effective than the standard OIV descriptor (Rist et al., 2019; Tello et al., 2016). In addition, laser scanners and depth cameras can achieve a complete reconstruction of bunch shape for the purpose of morphological study (Marinello et al., 2016; Rist et al., 2018).

Photogrammetry is a suitable technique for building digital models, also known as digital twins (DTs), of objects and environmental scenarios based on the structure through motion processes. According to Matthews (2008), close-range photogrammetry occurs if the target-to-camera distance is less than 300 m, and the procedure aims to increase the resolution of details in the final product. Photogrammetry is commonly based on multiple images acquired from the same targets, but captured from different angles. Thus, feature tracker algorithms, such as the Kanade-Lucas-Tomasi algorithm (Tomasi & Kanade, 1991), perform image alignment, providing depth and spatial information for each point in the DT reconstruction of objects at accurate scale dimensions. Schneider et al. (2020) set up a laboratory trial to investigate bunch morphology and feature prediction for future in-field adoption. Herrero-Huerta et al. (2015) and Rose et al. (2016), attempted to estimate yield components by taking photos directly in the field. Additionally, Torres-Sánchez et al. (2021) investigated the point cloud generated by photogrammetry from a vineyard monitored by a for yield estimation.

The current study explores a three-dimensional DT analysis as a deep analysis of grapevine bunch morphology. The DTs of several Pinot Gris and Pinot Noir bunches were constructed with photogrammetry techniques. A commercial camera was used to collect photos of the bunches. Cameras and photogrammetry represent inexpensive and ready-to-use tools for constructing accurate, high-resolution DTs. After construction, each DT was investigated to identify alternative descriptors to estimate the grey mould infection risk. Finally, a multiple linear regression model (MLR) was tested to identify which descriptors were most related to the grey mould severity assessed in the field. Because the standard bunch assessment often fails to detect slight differences between the morphology of clones from the same variety, this study aimed to categorise objective measures related to compactness and bunch rot susceptibility.

2. Materials and methods

DT modelling was performed on twenty-three grapevine clones from two grapevine cultivars (Pinot Gris and Pinot Noir) susceptible to grey mould bunch rot. A standardised methodology was employed to assess the spread of *Botrytis cinerea* in the field while images were acquired in a fixed environment. Due to a lack of in-season data on Pinot Noir, two methodologies were used to assess *Botrytis cinerea* severity among clones. In the following paragraphs, each of these steps is presented.

2.1. Grape bunches

The grape bunches came from two varietal collections. The first Pinot Gris vineyard was located in Cimadolmo (Treviso, Italy – 45°47′33.78″N, 12°20′30.22″E), while the Pinot Noir vineyard was located in San Michele all'Adige (Trento, Italy – 46°11′42.42″N, 11°8′16.28″E). More specifically, 105 healthy bunches of 17 Pinot Gris clones were manually gathered on August 21, 2020, by the CREA-VE of Conegliano researchers, while 33 healthy bunches of six Pinot Noir clones were

gathered on September 14, 2021, by researchers of the Laimburg Research Centre. All the Pinot bunches were harvested at the "berries ripe for harvest" phenological BBCH stage (BBCH 89). Clones were numbered following an arbitrary classification; Tables 1 and 2 resume the corresponding clone's name and number. The severity of grey mould in the vineyard was evaluated on Pinot Gris on the same harvesting day by evaluating 150 bunches from each clone. The bunches were rated using an arbitrary scale ranging from 0 to 3 based on the extent of the mould on the bunch surface, with 0 indicating no symptoms, 1 indicating from 1 to 25%, 2 indicating from 26 to 50%, and 3 indicating more than 50%. Then, the Townsend-Heuberger index (TH) was computed, giving a score to each clone ranging from 0 to 100. Eq. (1) (Townsend & Heuberger, 1943) is as follows:

$$TH = \frac{\sum_{1}^{i} (Ni * Vi)}{N * V} \quad (1)$$

where TH is the Townsend-Heuberger index, Ni is the number of grape bunches in each class, Vi is the class of grey mould infection, N is the total sampled bunches, and V is the highest class value. More details about the grey mould spread on the Pinot Gris bunches are shown in Fig. A1. The TH index retrieved a continuous ranking. Hence, the clones were grouped into classes to obtain practical insights into the grey mould risk of each one based on the dataset information. The number of classes was determined as suggested by Sturges (1926) following Eq. (2):

$$Cl = 1 + (10 * 3^{-1}) * \log N \quad (2)$$

where Cl is the optimal class number and N is the number of samples.

In Pinot Noir, clones were rated in ten classes by tolerance to *Botrytis cinerea* according to historical data gathered by the Laimburg Research Centre (Terleth & Pedri, 2010). The classes ranged from 1 to 10, and in this paper, the bunches were also classified from low to very high resistance against grey mould. All the bunches were categorised following the OIV standards, and the number of wings, height, width, shape, and average grape weight of clusters were measured. Additionally, the bunches were weighed, and the volume was determined using the water displacement method. The Ravaz index was calculated for Pinot Gris to compare the plant vigour among the clones by weighing the fresh pruning wood and the fruit production in fifty vines per clone. The Ravaz index was computed as the ratio between the fruit yield and the pruning wood weight (Ravaz, 1911). Tables 3 and 4 reassume Pinot Gris and Pinot Noir features.

Table 1
Conversion between Pinot Gris clone names and code used in this article. The column "Class" refers the to Sturges' classification of bunch rot according to the in-field evaluation.

Clone Name	Code	Class	Clone Name	Code	Class
B 10	PG-4	Very High	R 6	PG-6	Medium
H-1	PG-5	Very High	SMA 514	PG-10	Medium
VCR-5	PG-12	Very High	ENTAV 457	PG-1	Low
FENDIT 13-CSG	PG-14	Very High	SMA 505	PG-3	Low
CRAVIT ERSA 152	PG-9	High	ENTAV 52	PG-7	Low
ERSA FVG 151	PG-13	High	ISV-F1 TOPPANI	PG-11	Low
ENTAV 53	PG-15	High	FR 49-207	PG-16	Low
ISMA-AVIT 513	PG-17	High	1 GM	PG-8	Very Low
2–15 GM	PG-2	Medium			

Table 2
Conversion between Pinot Noir clone names and code used in this article. The column "Class" refers to the bunch rot resistance according to the Laimburg Research Centre studies.

Clone Name	Code	Class
828	PN-3	Low
SMA-201	PN-5	Low
165	PN-1	Medium
667	PN-6	Medium
583	PN-2	High
GM-2013	PN-4	Very High

2.2. Image collection and analysis

Once collected, the bunches were stored in boxes and preserved in a refrigerator. A series of photos were taken per bunch under laboratory conditions in a dark room lit by neon and LED lights. A Nikon D5100 camera (Nikon Corporation, Tokyo, Japan) with a focal length of 35 mm was used to take the photos. The camera captured coloured images at a 24-bit resolution of 4928x3264 pixels and saved the photos in JPG format. The bunches were hung while the camera was mounted to a special device that turned around the target at a constant rotation speed. The distance between the camera and the bunch was set constantly at approximately 450 mm. The camera took a picture every 2 s thanks to the multi-shot function while rotating. The rotation speed was set to 33 images per revolution (360°). The camera was mounted at three different positions: I) perpendicular to the bunch's vertical axis; II) at +45° from the perpendicular position; and III) at −45° from the perpendicular position. The acquisition from a different point of view allowed the complete representation of the clusters. As a result, 99 images were captured per bunch.

The background was excluded thanks to a white panel behind the cluster. The device is shown in Fig. 1(a). All photos were processed on Metashape 1.7.2 (Agisoft LLC) to build the DT of each bunch. Metashape can generate DTs of real objects by performing the structure from motion photogrammetry of digital images. The specific functions used for this purpose are summarised in Table 5. A calibration artefact with known dimensions and shape was captured as a reference to allow calculation of first- and second-degree correction factors (Marinello et al., 2009) and following compensation of systematic scaling and crosstalk errors during the grape 3D reconstruction process. Finally, the artefacts from the background were quickly deleted by hand.

2.3. 3D analysis

All workflow settings were adjusted to reach the highest quality DT. The obtained DTs are faithful to real bunches. On average, the point clouds were made by 224.46 points per mm^2, while the meshes counted, on average, 44.89 faces per mm^2. The smallest curvature radius measured between grapes was 0.2 mm. All the items owned neither to the bunch nor the wood cube were classified as "background noise". However, the background noise did not affect the DT quality. On average, only 2976.13 faces were classified as "background noise" and manually deleted from the bunches' meshes. The depth resolution was closely related to the bunch compactness and lighting. As shown in Fig. 8, the rachis was visible in the loosest bunches, while two LED bulbs emitting 460 lm light avoided any shadowing interference.

The 3D analysis continued examining the DTs. CloudCompare (www.cloudcompare.org) was used to extract five horizontal sections perpendicular to the bunch's vertical axis and to measure the bunch's surface and the whole mesh's volume (Fig. 1(b)). The sections cut the cluster from the top to the bottom of the bunch's height at 16.67%, 33.33%, 50%, 66.67%, and 83.33%. Fig. 2 shows in detail the position of the sections. Two vertical sections were extracted. The first was positioned according to the bunch's maximum width, while the second was perpendicular to the first. The sections reflected the bunch's profile

Table 3
The table presents Pinot Gris bunches' classification according to the OIV standard. The average and the standard deviation of the bunch's main features are also listed. The "Shape" column describes the whole bunch structure, where C indicates a cylindrical shape, F is a funnel shape, and CF indicates bunches have both shapes. In this table, TH ranged from 4.44 to 14.98, where the lower values indicate low grey mould infections, while higher values indicate a strong presence.

Clone	Samples N°	Wings	Shape	Weight (g)	Volume (mm^3) *10^3	Height (mm)	Width (mm)	Berries N°	TH	Ravaz Index
PG-14	6	1.0	C	149.4 ± 16.8	142 ± 16	140 ± 7	104 ± 5	109.7 ± 5.5	14.9 ± 3.4	11.5 ± 1.5
PG-12	6	1.0	C	166.3 ± 32.2	163 ± 35	121 ± 11	87 ± 9	97.7 ± 5.6	13.8 ± 1.0	8.2 ± 1.9
PG-5	7	1.0	C	213.6 ± 27.8	193 ± 21	133 ± 13	91 ± 9	76.9 ± 5.3	13.3 ± 1.3	4.5 ± 0.5
PG-4	7	1.0	C	178.9 ± 17.9	174 ± 19	124 ± 1	81 ± 46	112.7 ± 5.3	12.7 ± 2.9	11.7 ± 4.3
PG-13	6	1.0	C	147.6 ± 9.8	137 ± 10	140 ± 12	95 ± 12	111.9 ± 5.4	12.4 ± 3.0	11.8 ± 5.5
PG-9	5	1.0	CF	166.5 ± 14.4	150 ± 17	144 ± 4	74 ± 10	101.9 ± 5.0	11.6 ± 2.8	7.5 ± 2.8
PG-17	4	1.0	CF	149.1 ± 12.1	143 ± 15	121 ± 13	110 ± 3	129.3 ± 6.6	11.6 ± 3.7	12.1 ± 6.0
PG-15	7	1.0	C	172.5 ± 18.1	157 ± 22	126 ± 8	81 ± 2	98.1 ± 5.3	11.1 ± 2.7	12.2 ± 2.6
PG-6	5	1.0	C	172.2 ± 24.7	155 ± 24	129 ± 8	78 ± 8	103.8 ± 4.0	10.4 ± 3.8	9.1 ± 1.4
PG-2	7	1.0	C	178.3 ± 34.4	170 ± 31	122 ± 1	81 ± 4	117.0 ± 5.3	9.8 ± 3.0	13.9 ± 1.9
PG-10	7	1.4	CF	189.7 ± 38.2	173 ± 37	134 ± 3	132 ± 5	96.7 ± 5.3	9.1 ± 2.0	12.9 ± 3.5
PG-11	7	1.0	C	168.8 ± 26.0	159 ± 22	122 ± 10	81 ± 12	102.2 ± 5.3	8.4 ± 2.5	8.2 ± 2.9
PG-1	7	1.0	CF	186.7 ± 30.1	180 ± 30	141 ± 11	75 ± 9	101.3 ± 5.4	8.0 ± 3.5	9.6 ± 1.0
PG-16	7	1.0	F	234.6 ± 31.9	221 ± 33	150 ± 2	68 ± 6	109.1 ± 5.2	7.3 ± 0.7	7.8 ± 2.4
PG-7	5	1.0	F	203.4 ± 33.3	184 ± 32	150 ± 11	78 ± 6	110.6 ± 6.1	6.9 ± 1.5	10.6 ± 1.3
PG-3	7	1.0	C	161.4 ± 16.2	156 ± 15	128 ± 7	79 ± 8	101.8 ± 5.0	6.7 ± 1.2	12.8 ± 5.2
PG-8	6	1.2	F	238.0 ± 30.6	217 ± 23	163 ± 12	69 ± 9	140.4 ± 4.9	4.4 ± 1.4	17.3 ± 4.6

Table 4
The table presents Pinot Noir bunches' classification according to the OIV standard. The average and the standard deviation of the bunch's main features are also listed. The "Shape" column describes the whole bunch structure, where C indicates a cylindrical shape, F is a funnel shape, and CF indicates bunches have both shapes. The class ranged from "Low" to "Very High", where "Very High" indicates the most resistant, while "Low" indicates the most susceptible.

Clone	Samples N°	Wings	Shape	Weight (g)	Volume (mm^3) *10^3	Height (mm)	Width (mm)	Berries N°	Class
PN-3	5	1.0	C	211.8 ± 60.8	178 ± 54	141 ± 17	86 ± 13	109.4 ± 34.1	Low
PN-5	6	1.0	C	146.1 ± 12.9	123 ± 5	127 ± 9	78 ± 8	92.7 ± 7.4	Low
PN-1	6	1.0	CF	406.0 ± 55.2	132 ± 10	129 ± 18	80 ± 12	93.0 ± 17.0	Medium
PN-6	4	1.0	C	209.7 ± 17.7	193 ± 10	147 ± 10	80 ± 2	102.6 ± 37.7	Medium
PN-2	6	1.0	C	114.8 ± 41.2	132 ± 84	124 ± 11	76 ± 15	96.5 ± 35.5	High
PN-4	6	2.0	C	171.8 ± 36.8	148 ± 42	139 ± 10	109 ± 12	115.3 ± 27.0	Very High

containing, on average, 7.10 vertices per mm.

AutoCAD 2022.1 (Autodesk) was used to measure the perimeter, area, and axis length of all the sections. In addition, the circumscribed circle of all the horizontal sections has been drawn (Fig. 1(c)). Finally, 61 parameters were calculated among the direct measures and derived indices (Table 6).

2.4. Statistical analysis

Some parameters were replicated in each horizontal and vertical section, so the bunch evaluation retrieved 82 direct measures and 103 derived indices from each bunch. Feature selection was carried out to reduce the number of variables and to identify the variables most related to the grey mould infection risk. First, a principal component analysis (PCA) was carried out on direct measures and derived indices separately. Next, the loading value of each variable was compared among the components explaining at least 88% of the total variance. Then, a correlation matrix was computed to detect the most autocorrelated variable. Finally, the most prominent and less autocorrelated variables were included in a dataset to propose an MLR for grey mould severity estimation. A forward stepwise regression was used for selecting models with the lowest Akaike Information Criterion (AIC) value and the smallest number of variables to avoid overfitting the model (Chaurasia & Harel, 2012). The first included only information reachable from a common two dimensions (2D) analysis, while the second included information from the third dimension. The maximum number of features that showed a significant contribution to the model was considered (p value ≤ 0.05). Because disease severity was available as the clone mean, all bunch features were averaged among the same clone for the regression study. Finally, the model's square regression coefficient (R^2) and the root mean square error (RMSE) were compared between the models' prediction and the actual disease severity index. RStudio (version 1.2.1335 © 2009-2019 RStudio) was the software chosen for statistical analysis.

3. Results

Table 7 reassumes the weather data recorded by the closest weather station in Cimadolmo (45°48′5.86″N, 12°20′26.18″E) during vintage 2020 compared to the historical records between 1994 and 2019. July and August 2020 were warmer and rainier than the historical trend. Pinot Gris' veraison occurred in the third week of July. Therefore, the rainfalls that occurred during the summer of 2020 might have promoted *Botrytis cinerea* infections against the most sensitive clones.

The chart in Fig. 3 displays the scores of the Pinot Gris bunches among the first and second PCA dimensions. In this case, the PCA considered the direct measures. The first and second dimensions explain 33.58% and 20.10% of the total variance, respectively. The data were grouped by clone number, while the point's colour represented the grey mould severity class listed in Tables 1 and 2. First, the bunches of clones PG-1, PG-5, and PG-12 are clustered in the same chart area. Other clones, for instance, PG-3, PG-9, and PG-10, are much more widespread. PG-8 is the only clone assigned to the lowest class, and all the bunches are clustered in the bottom right corner of the chart. Most of the "Low" class clones (green points) are close to the bottom right corner, while most of the clones assigned to the Very High class are clustered in the top left corner. Additionally, in the central part of the chart, there is a clear diagonal trend from the bottom right to the top left corner.

The PCA that was conducted for Pinot Noir clustered most of the bunches of clone PN-4 on the bottom right corner of the chart in Fig. 4. Although the rest of the classes are more blended than what happened for Pinot Gris, the same diagonal trend is preserved from the bottom right corner to the top left corner. As verified in Pinot Gris, the clones of the lowest and the highest class occupy opposite corners.

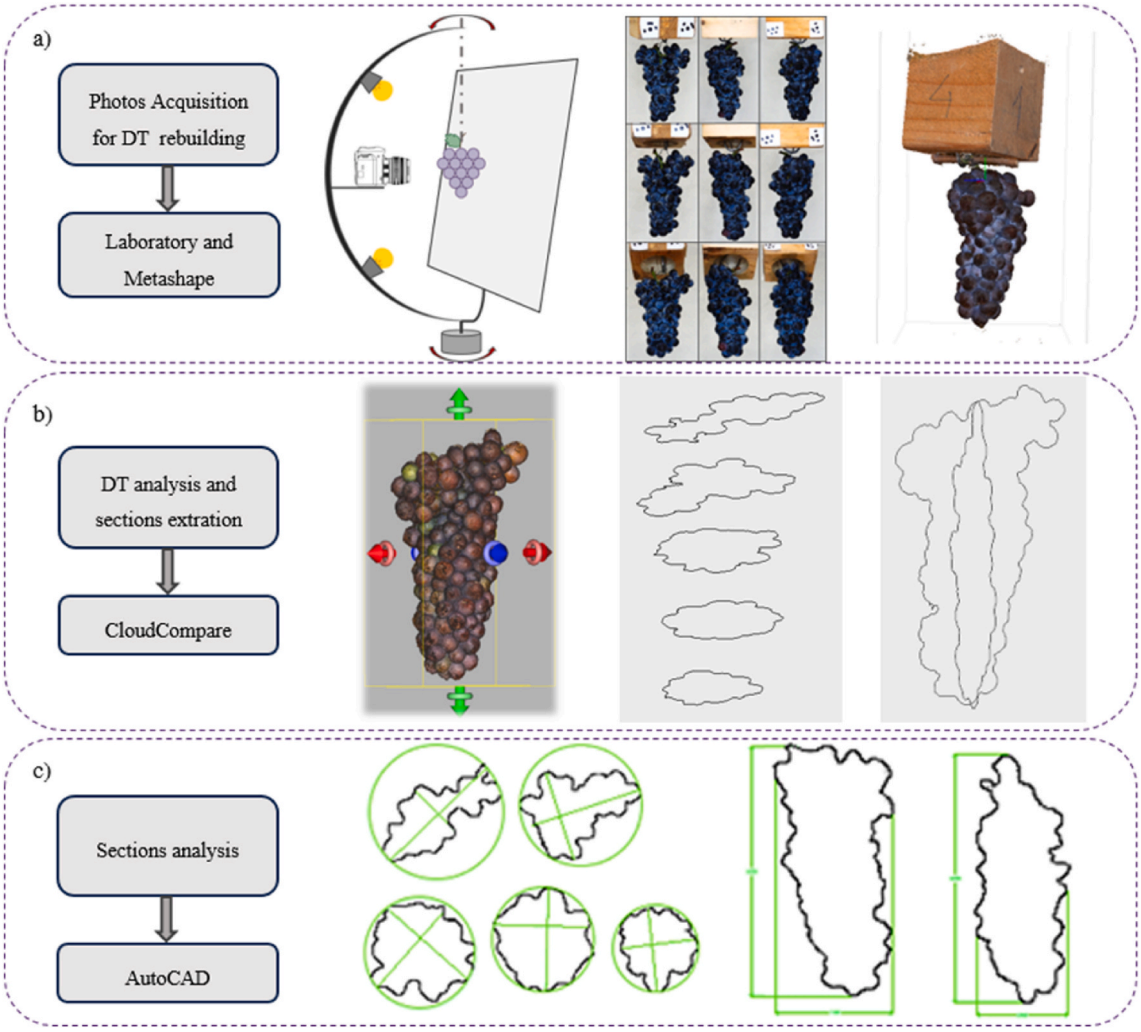

Fig. 1. The above pictures explain the whole sequence of operations performed. In a) the devices used to take the photos and some examples of bunch photos are presented; b) the DTs were built from the photos processed, and the sections were extracted; c) finally, the sections were analysed.

Table 5
Here, the sequences of operations performed on Metashape are presented to build the DT of the bunches from a series of photos.

Function	Description
Align Photos	The software estimates the camera actual position ed projects a sparse point cloud.
Optimise Camera Alignment	It adjusts the point coordinates estimated, minimising reprojection and misalignment errors.
Build Dense Cloud	The software computes the spatial coordinates of all the points those made the bunch and projects a high-resolution point cloud.
Build Mesh	Metashape can join all the point cloud's vertices reconstructing the external surface of the bunch; each mesh's point colour is estimated by the original photos.

The 2D regression model considered only features measured directly on bunches and all those features reachable by 2D image analysis (Chen et al., 2018; Tello et al., 2016). On the other hand, the 3D regression model exploited all the 2D information and the measurements given by section analysis, volume and the surface of the DT. Both direct measures and indices were considered for the regression analysis. The same number of features were considered in the 2D and 3D models, avoiding the overfitting effect by considering a different number of variables. Variables used in the models were selected according to the model evaluation metrics (AIC) test. In Pinot Gris, five descriptors were enough

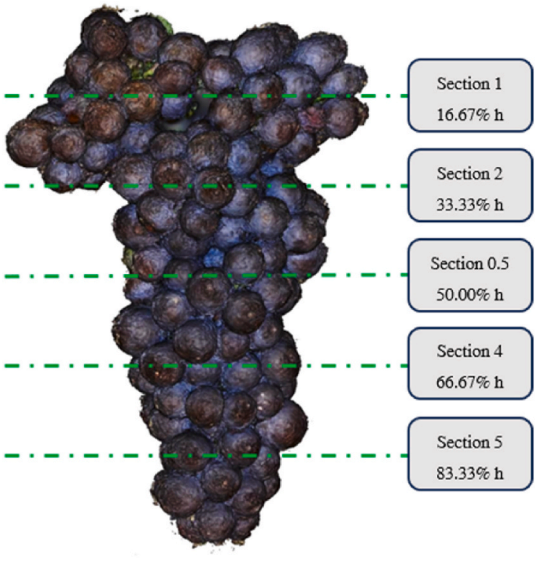

Fig. 2. Details of the horizontal sections.

Table 6
The table lists all the direct measures and derived indices measured in each grape. Some parameters were measured or calculated in several sections. The column on the left contains the abbreviations for the measures and indices. The reference indicates the citation, and "***" indicates which measures were proposed in this study. Empty cells indicate general geometry rules. The "Object" column aims to specify which object was measured, "H" indicates horizontal section, "V" indicates vertical sections, "DT" indicates the bunch's digital twin, and "Bunch" indicates the original cluster.

Measure	Reference	Formula	Object	Description	Unit
Direct measures					
P			H, V	Perimeter of horizontal (1,2,0.5,4,5) or vertical (x, z) sections	mm
A.			H, V	Area of horizontal (1,2,0.5,4,5) or vertical (x, z) sections	mm^2
Cm	Bribiesca (2008)		H	Perimeter of the circumference which has the same area as the horizontal section.	mm
P_Ccirc	Li et al. (2013)		H	Perimeter of the smallest circumference containing the section	mm
AC	Li et al. (2013)		H	Area of the smallest circumference containing the section	mm^2
Ø_Ccirc	Li et al. (2013)		H	Diameter of the smallest circumference containing the section	mm
Mj_a			H	Major axis is the longest line that can be drawn inside a horizontal section	mm
mn_a			H	Minor axis is the longest line perpendicular to the major of horizontal sections	mm
P_diff	***	P - P0.5	H	Difference between horizontal section's perimeter (1,2,4,5) and the middle section's perimeter	mm
A_diff	***	A - A0.5	H	Difference between horizontal section's area (1,2,4,5) and the middle section's area	mm^2
h	OIV (2009)		V, DT	Bunch's height	mm
hx, hz	***		V	Height of vertical (x,z) sections	mm
W_bunch	OIV (2009)		Bunch	Maximum bunch's width	mm
W	***		H, V	Width of horizontal (1,2,0.5,4,5) or vertical (x, z) sections	mm
Bb_V	***	H * W * Wz	DT	Volume of the bunch's bounding box	mm^3
Bb_S	***	2* (h * Wx + h * Wz + Wx * Wz)	DT	Surface of the bunch's bounding box	mm^2
Dt_V	***		DT	Volume of the DT computed on CloudCompare	mm^3
Wgt	OIV (2009)		Bunch	Bunch's weight	g
AcV	OIV (2009)		Bunch	Actual volume of the bunch measured with the water displacement method	mm^3
EV	***	Dt_V - AcV	DT	Empty volume is obtained by the difference between the computed and the actual bunch's volume.	mm^3
DtS	***		DT	Surface of the DT computed by CloudCompare	mm^2
NB	***		H	Number of berries in the middle horizontal section	berry
CsV	***		H	Volume of the convolutional solid containing the whole bunch	mm^3
CsS	***		H	Surface of the convolutional solid containing the whole bunch	mm^2
AbWgt	OIV (2009)		Bunch	Average berries weight	g
TotB	Tello et al. (2015)		Bunch	Total number of berries per bunch	berry
Derived indices					
AP	Cubero et al. (2015)	$A * P^{-1}$	H, V	Ratio between the area and perimeter of horizontal (1,2,0.5,4,5) or vertical (x, z) sections	mm
PA	Li et al. (2013)	$P * A^{-1}$	H, V	Ratio between perimeter and area of horizontal (1,2,0.5,4,5) or vertical (x, z) sections	mm^{-1}
EC	Zhang and Lu (2004)	$Mj\_a * mn\_a^{-1}$	H	Axis ratio of horizontal (1,2,0.5,4,5) or vertical (x, z) sections	
PAc	***	$P * Cm^{-1}$	H	Ratio between the section perimeter and the area of the median circumference	mm^{-1}
APc	***	$A * Cm^{-1}$	H	Ratio between the area of the section and the perimeter of the median section	mm
CFS	Cubero et al. (2015)	$(P^2 * A^{-1}) * \pi^{-1}$	H, V	Ratio between the section's perimeter and area, circle = 4. Higher values indicate more compactness.	mm^{-1}
RD	Cubero et al. (2015), Li et al. (2013)	$(4 * \pi * A) * P^{-1}$	H	Ratio between the section's area and perimeter, a circle, has the highest value = 1.	mm
Cdcm	Li et al. (2013)	$A * Asc^{-1}$	H	Ratio between the section area and the area of the smallest circumference containing the section	
Comp	Bribiesca (2008)	$Cm * P^{-1}$	H	Ratio between the perimeter of the median circumference and the section's perimeter.	
ACisoA	***	$A * \pi\text{-}1 * (P * (2 * \pi)^{-1})^2$	H	Ratio between the area of the section and the area of the circumference having the same perimeter.	
Rar.	Chen et al. (2018)	$A * (h * W)^{-1}$	V	Ratio between the vertical section area (x, z) and the area of the smallest rectangle containing the section.	
PP0.5	***	$P * P0.5^{-1}$	H	Ratio between the section's perimeter and the middle section's perimeter	
AA0.5	***	$A * A0.5^{-1}$	H	Ratio between the section's area and the middle section's area	
Rr	Chen et al. (2018)	$H * W^{-1}$	DT	Ratio between the vertical section orthogonal dimension	
P0.5NB	***	$NB * PH0.5^{-1}$	H	Ratio between the perimeter of the middle section and the number of berries in that section	$mm * berry^{-1}$
A0.5NB	***	$NB * AH0.5^{-1}$	H	Ratio between the area of the middle section and the number of berries crossed by the same section	$mm^2 * berry^{-1}$
Cm0.5NB	***	$NB * CmH0.5^{-1}$	H	Ratio between the Cm of the middle section and the number of berries crossed by the same section	$mm * berry^{-1}$
AC0.5NB	***	$NB * ACH0.5^{-1}$	H	Ratio between the AC of the middle section and the number of berries crossed by the same section	$mm^2 * berry^{-1}$
AS	Cubero et al. (2015)	$Wx * H^{-1}$	DT	Ratio between the bunch's width (the widest) and its height	
Ef	***	$EVol * Dt\_V^{-1}$	DT	Ratio between the empty volume and the computed volume	
AcV_BV	***	$AcV * BV^{-1}$		Ratio between the actual bunch's volume and the volume of the smallest solid containing the whole bunch	
VRr	***	$Dt\_V * BV^{-1}$	DT	Ratio between the DT volume and the volume of the smallest solid containing the whole bunch	
VCRr	***	$(Dt\_V * \pi^{-1} * h^{-1}) * (Wx * 0.5)^2$	DT	Ratio between the bunch's volume and the volume of the smallest cylinder containing the whole bunch	

(*continued on next page*)

Table 6 (*continued*)

Measure	Reference	Formula	Object	Description	Unit
Rpr	***	$S * BS^{-1}$	DT	Ratio between the bunch surface and the surface of the smallest bounding box, the whole bunch	
Cvol	***	$S * Dt\_V^{-1}$	DT	DT surface and volume ratio, perfect cube = 1.	mm^{-1}
Density		$Wgt * AcV^{-1}$	Bunch	Ratio between the bunch's weight and apparent volume.	$g * mm^{-3}$
AcVh	OIV (2009)	$Dt\_V * h^{-1}$	DT	Ratio between the bunch's actual volume and height	mm^2
Dt_V h	***	$Dt\_V * h^{-1}$	DT	Ratio between the DT's volume and height	mm^2
Sh	***	$S * h^{-1}$	DT	Ratio between the DT's surface and height	mm
ECsV	***	CsV - Dt_V	DT	Difference between the convolutional solid containing the whole bunch and the DT's volume	mm^3
FCsV	***	$CsV * Dt\_V^{-1}$	DT	Ratio between the convolutional solid containing the whole bunch and the DT's volume	
SCsV	***	$S * CsV^{-1}$	DT	Ratio between the DT surface and the volume of the convolutional solid containing the whole bunch	mm^{-1}
ETotB	***	$Evol * TotB^{-1}$	DT	Ratio between the bunch's empty volume and the total number of berries	$mm^3 * berry^{-1}$
CsVTotB	***	$CsV * TotB^{-1}$	DT	Ratio between the volume of the convolutional solid containing the whole bunch and the total bunch's berries	$mm^3 * berry^{-2}$
STotB	***	$S * TotB^{-1}$	DT	Ratio between the DT's surface and the total berries number	$mm^2 * berry^{-2}$

to describe the MLR proposed for 2D analysis. According to the statistical analysis, adding another variable could increase the model fitting without proving any significant improvement (Table A1). Eqs. (3) and (4) reveal the 2D and 3D models, respectively. The models aimed to predict the disease severity index (TH), and the models' performance was compared to the actual TH indices for Pinot Gris. The R^2 rose from 0.656 to 0.838, while the RMSE decreased from 1.713 to 1.175 by joining 3D to the 2D information. AcV_BV and W_bunch depend on the presence of wings on the bunch (lateral branch with berries). W0.5 and W1 indicate the maximum bunch width at the middle and first sections closest to the peduncle, respectively, and they were related to the bunch shape. Empty volume (EV) was estimated by the difference between the total volume of the DT mesh (Fig. 1) and the bunch's actual volume (AcV), which only considers the volume of berries and rachises.

Table 7
Monthly mean temperature and total rainfall of 2020 vintage compared to the historical data recorded by the closest weather station.

Period	Value	April	May	June	July	August
2020	Mean Temp. (°C)	9.9	18.2	21.2	24.0	24.6
Historic	Mean Temp. (°C)	13.0	17.7	21.6	23.4	22.9
2020	Rainfall (mm)	27.8	118.8	204.0	100.4	196.6
Historic	Rainfall (mm)	101.4	124.8	106.8	90.6	103.9

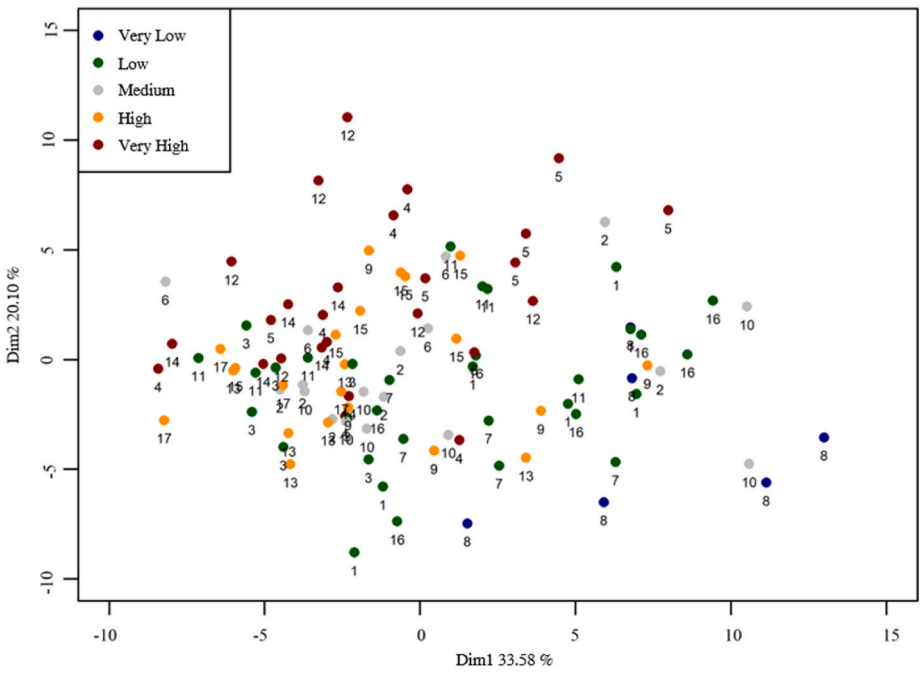

Fig. 3. The scatter plot shows Pinot Gris PCA bunches' scores distributed according to dimensions one (Dim1), horizontal axis, and two (Dim2), the vertical axis. The points represent all the bunches sampled. The numbers indicate the clone. The clone's name and number are listed in Table 1. The colour indicates the severity class. Numbers 33.58% and 20.10% represent the portion of total variance explained by the first and the second PCA dimensions. (For interpretation of the references to colour in this figure legend, the reader is referred to the Web version of this article.)

Therefore, the empty fraction (Ef) was computed as the ratio between EV and AcV. Sh is the ratio between the mesh surface and the bunch height. Mj_A_1 and Mj_A_4 indicate the length of the longest axis of sections one and four, at 16.67% and 66.67% of the bunches' height, respectively. The scatter plots in Fig. 5 display the clones among actual and predicted TH values, while the colour indicates the severity class assigned to clones.

In Pinot Noir, the MLR estimated the resistance class against grey mould. Any descriptors of the 2D model did not prove any significant contribution. Therefore, the MLR computed on the 3D descriptor included three variables (Eq. (5)), which was the best MLR among all the combinations of variables, avoiding overfitting. As a result, the proposed MLR estimated an R^2 of 0.936 and an RMSE of 0.297. The scatter plot in Fig. 6 displays the clones in relation to actual and predicted resistance, while the colour indicates the severity class assigned to the clones. In Eq. (5), P0.5NB is the ratio between the perimeter and the number of berries counted in the middle horizontal section, while CsS is the surface of the convolutional solid containing the bunch.

$$TH = -32.8236 *AcV\_BV -16.4542 *W0.5 + 0.0743 *W\_bunch -0.4630 *h -0.3148 *W1 +38.864 \quad (3)$$

$$TH = -4.8797 *Ef+0.4142 *Sh-2.4653 *P0.5NB -0.6864 * Mj\_A\_4–3.570 * Mj\_A\_1 + 32.6925 \quad (4)$$

$$Grey\ Mould\ Resistance = 8.1643 *P0.5\ NB +0.7079 * Mj\_A\_4 + 25.1527 *CsS -30.8111 \quad (5)$$

4. Discussion

The contributions of value in the present research are twofold: the development of the reconstruction and analysis method and the agronomical impact of the results.

4.1. Instrumental approach

The physical distribution of grape volume is traditionally correlated with the severity of the attack of some diseases for a given variety. Properly characterising the shape of grapes requires taking both the instrument and subsequent data processing into consideration. The present study showed the ability of photogrammetry to properly reconstruct complex three-dimensional bunch shapes. Of course, 3D reconstruction is highly demanding in terms of data processing as well as high-density point cloud handling. For this reason, most of the research in recent years has focused on depth cameras, mainly taking advantage of disparity maps or time of flight for 3D reconstruction. 3D photogrammetry benefits from the high performance of computers reached in recent years. For example, 5–7 h were needed for a shape made by 19 million points. Hence, interest in photogrammetry has increased since 3D photogrammetry for the above-mentioned issues and many other reasons. For instance, photogrammetry is of great help to support steering systems or automated machinery (van Marrewijk et al., 2022). Additionally, photogrammetry was employed for automated plant phenotyping, fruit detection, and localisation techniques (Boogaard et al., 2023; Rapado-Rincón et al., 2023). Finally, the mean root square roughness measured 12.523*10-3 mm on an almost "smooth" surface. Hence, for such highly accurate detail, sophisticated photogrammetry could be less affordable than a more sophisticated 3D scanner (Moreau et al., 2014).

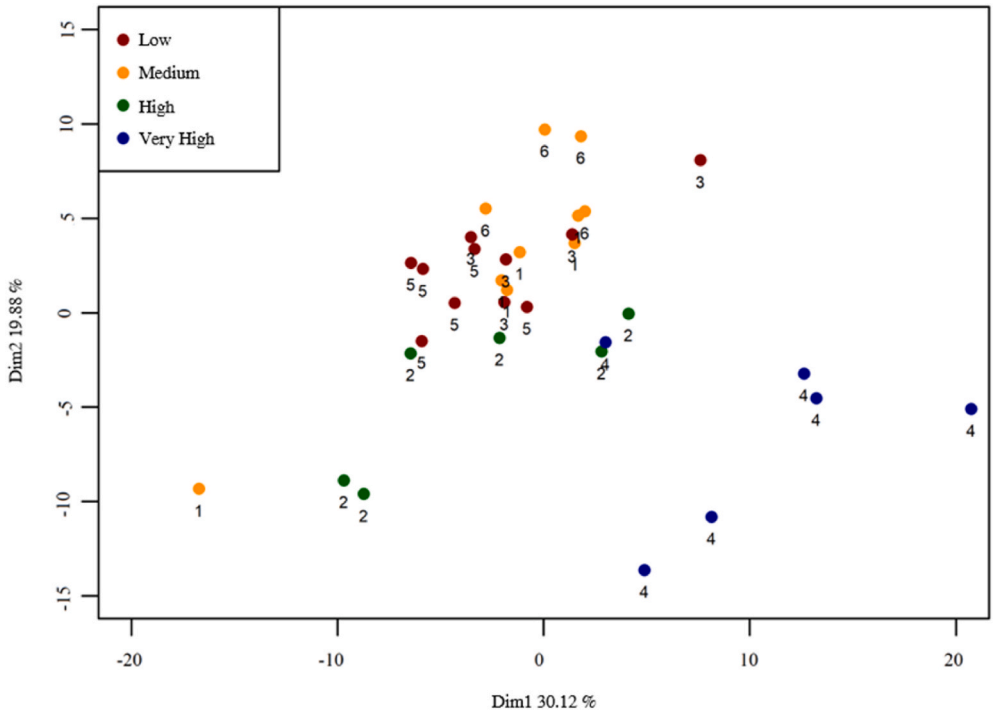

Fig. 4. The scatter plot shows that Pinot Noir PCA bunch scores are distributed according to dimensions one (Dim1), horizontal axis, and two (Dim2), vertical axis. The points represent all the bunches sampled. The numbers are referred to as clones. Clones' names and numbers are listed in Table 2. The colour indicates the resistance class against the grey mould. Numbers 30.12% and 19.88% represent the portion of total variance explained by the first and the second PCA dimensions. (For interpretation of the references to colour in this figure legend, the reader is referred to the Web version of this article.)

4.2. Agronomical results

The score plotting from PCA identified a diagonal trend crossing the second and fourth quadrants in Pinot Gris and Pinot Noir. The PCA was carried out only on direct measures because these parameters explained much more variance than indices. More specifically, because indices come from direct measures, they are autocorrelated. The PCA charts did not return the same results found by Cubero et al. (2015), where authors compared grapevine varieties instead of clones. Regarding the PCA on Pinot Gris, clone PG-8 was attached to the lowest severity class, opposite from a group of clones assigned to the highest severity class, PG-14, PG-12, and PG-4. In addition, PG-8 was the longest and one of the widest clones, showing a funnel shape with two wings in many samples. PG-8 was the first clone for branching (AcV_BV) and estimated empty volume (EV)e and surface (DtS). All the previously mentioned features identified PG-8 as less compact than other clones (Fig. 7).

On the other hand, PG-14, PG-12, and PG-4 had a shape without any wings. They were among the shortest clones and had the smallest fraction of estimated empty volume and surface. As a result, clones PG-14, PG-12, and PG-4 were identified as a model of very compact bunches. Canopy leaf and shoot density promoted humidity and fungal attack on the grape bunches.

Therefore, the relationship between grey mould severity and the Ravaz index was investigated. Even though clone PG-8 showed the highest index value (Table 3), the linear regression between the Ravaz index and grey mould severity was meagre ($R^2 = 0.15$).

The Pinot Noir PN-4 clone was attached at the highest resistant class (the clone is the most tolerant against grey mould), and the PCA isolated those bunches from the other. PN-4 was the widest clone, with the largest surface having a cylindric shape and two wings. In addition, PN-4 was the second clone for the estimated empty volume fraction and branching. On the other hand, clones PN-3 and PN-5 were the least resistant to grey mould and were clustered with clone PN-6, which was assigned to the medium class. While PN-6 showed many descriptors of the middle classes, PN-5 was the smallest clone with the lowest value of the ratio between surface and height. Additionally, sections four and five were very tight, as verified in clone PN-3. However, the shape of the grape bunches was only one factor explaining the resistance or susceptibility to developing grey mould infections. For example, grape skin thickness, the chemical content of the grape juice, genetic patterns, destructive insects, the environment, and climate affect susceptibility to grey mould infection.

Following the OIV standard descriptor, it was impossible to find a strong relationship between the Pinot clone features and the severity of grey mould. This fact explains why all the bunches came from the same grapevine variety and were very similar. Almost all clusters were compact and cylindrical. Only a more detailed analysis could detect the smallest difference between clones.

Regarding Pinot Gris, R^2 increased, and RMSE improved in the 3D MLR compared to the 2D MLR. That happened considering the same number of variables, avoiding the overfitting of the model (Subramanian & Simon, 2013). The most prominent variables of the 2D MLR were the width of the sections, as stated by Underhill et al. (2020), and the presence of branching from the main body of the bunches. The section width is also included in the 3D MLR with many other interesting descriptors from the 3D analysis.

The mesh volume is consistently overestimated because it does not consider the empty space inside bunches. Therefore, the actual bunch volume and the mesh volume were used to estimate the space into a bunch, such as deduced by Tello et al. (2016). The same authors claimed the empty space as a relevant feature for describing the bunches morphology.

The ratio between the perimeter of the middle section and the berries number in the same section indicates the portion of the section perimeter occupied by each berry (Hed et al., 2009). Lower values could indicate that berries are tiny and compact. Fig. 9 shows an example of two wildly divergent clones. The clone PG-8 bunch has ten berries, while clone PG-14 has eleven ones and a smaller perimeter than clone PG-8. The ratio between the perimeter and berries was higher in favour of clone PG-8, at 20.837 and 17.854 mm * $berry^{-1}$, respectively.

The mesh surface depends on the bunch dimension, branching, and compactness. For example, the berries of compact bunches touched each other, while the berries of loose clusters were far from each other. As a result, the contribution of each berry in compact bunches to the whole

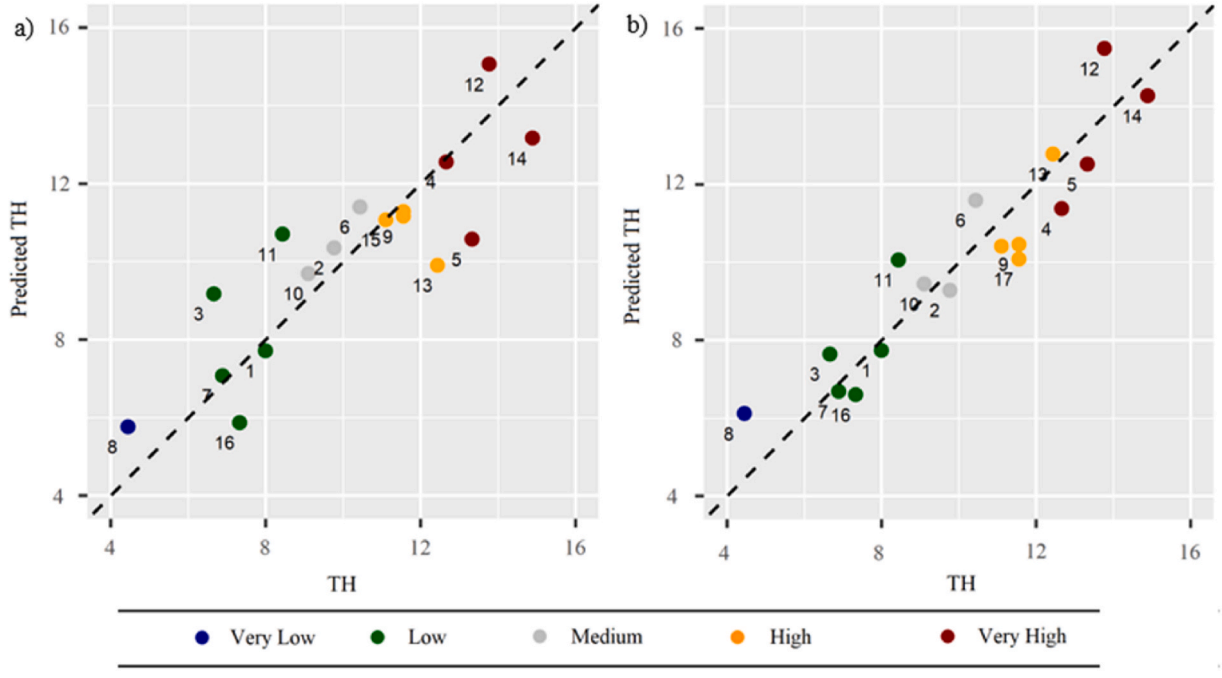

Fig. 5. The two scatter plots display the actual and predicted THs of Pinot Gris: a) 2D MLR and b) 3D MLR. The black line represents the ideal regression line with a slope value of 1, while the colour of the point refers to the clone severity class. (For interpretation of the references to colour in this figure legend, the reader is referred to the Web version of this article.)

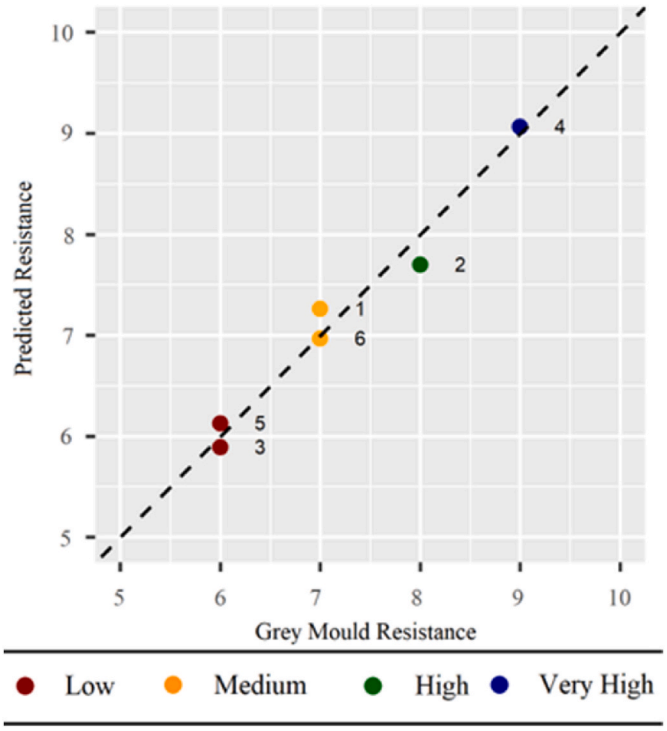

Fig. 6. The scatter plot displays the actual and predicted resistance against the grey mould of the 3D MLR model of Pinot Noir. The black line represents the ideal regression line with a slope value of 1, while the point's colour refers to as the clone resistance class. (For interpretation of the references to colour in this figure legend, the reader is referred to the Web version of this article.)

surface is lower than in loose bunches. The ratio between surface and height is an index that aims to standardise the surface to the cluster dimension. Similar results were found by Lopes and Cadima (2021) concerning bunch weight and compaction. However, the quality, resolution, and alignment of the photos could affect the surface measurements.

Regarding Pinot Noir, the 2D analysis failed because none of the 2D descriptors made a significant contribution to the MLR model. On the other hand, only three descriptors took part in the 3D MLR model. Compared to the Pinot Gris clone bunches, the Pinot Noir bunches were much more different, showing significant divergence in shape, number of wings, and branching (Fig. 8). The variability among clones could be a plausible explanation for the small number of variables included in Pinot Noir MLR. The relevance of CsS in the Pinot Noir MLR could be explained by the divergence between the clone shapes (Fig. A2).

In this study, bunch weight and volume were slightly relevant to predict bunch compactness and grey mould severity rather than stated by (Ivorra et al., 2015; Tello & Ibáñez, 2014). Indeed, the surface and the ratio between the bunch surface and height were strongly related to the bunch's compactness.

5. Conclusions

This work aimed to investigate the morphology of grapevine bunches using photogrammetry techniques for the whole DT reconstruction of grape bunches. Seventeen Pinot Gris clones and six Pinot Noir clones were compared to identify the most compact clone according to the spread of grey mould. All the DTs were processed using point cloud processing software, and five horizontal and two vertical sections were extracted. All the sections were analysed and hence compared. The PCA showed a distribution trend in the clone tendency to develop grey mould infections. Two MLRs were proposed per grapevine variety considering the most important descriptors for the bunch shape. The first model aimed to find the correlation between grey mould severity and the descriptors from the 2D analysis, while the second model also included descriptors from the 3D analysis. The 3D MLR showed higher performances than the 2D MLR. The proposed research demonstrated the relevance of cluster morphology to the susceptibility to grey mould infections. Future studies should validate the proposed models for the grapevine varieties and demonstrate the importance of the descriptors selected in this trial. Additionally, a completely automatic and unsupervised evaluation system based on artificial intelligence techniques could be developed.

Author contributions

Conception and design of methodology: **A. Zanchin, D. Giora, M. Sozzi**.

Acquisition of data: **A. Zanchin, D. Giora, Josef Terleth**.

Investigation and analysis of data: **A. Zanchin, M. Sozzi, M. Kalantari**.

Drafting the manuscript: **A. Zanchin, N. Belfiore**.

Revising the manuscript: **F. Marinello, N. Belfiore, D. Tomasi**.

Fig. 7. The pictures provide examples of Pinot Gris bunches. The first bunch on the left represents clone PG-8, showing a typical funnel shape. The second bunch is clone PG-13, which has two wings. PG-11 and PG-12 are the last two clones showing a cylindrical shape. Clone PG-11 has larger berries than PG-12 and PG-11 seems less compact than PG-12.

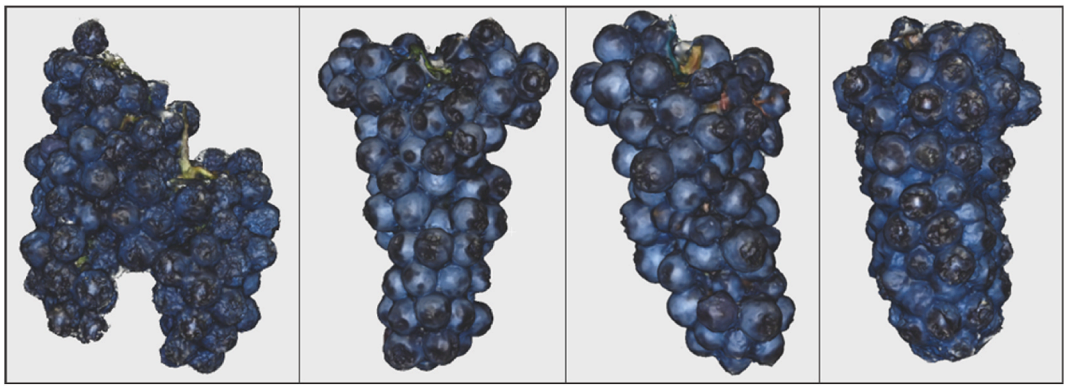

Fig. 8. The pictures provide examples of Pinot Noir Bunches. The first bunch on the left represents clone PN-4 split into two main branches. The second clone is PN-5, showing a funnel shape. The last two images refer to clones PN-2 and PN-3, showing a cylindrical shape. Clone PN-2 has larger berries than PN-3. Also, PN-2 seems less compact than PN-3.

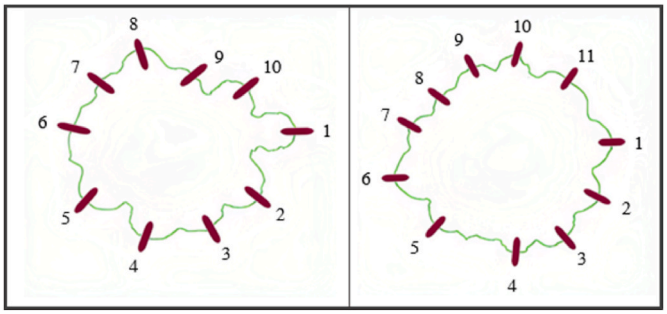

Fig. 9. The picture shows an example of two horizontal middle sections of different bunches. Clone PG-8 is on the left, while PG-14 is on the right. PG-8 counts ten berries, and the section's perimeter measures 200.837 mm, while PG-14 counts 11 berries, and the section's perimeter measures 196.397 mm.

Declaration of competing interest

The authors declare that they have no known competing financial interests or personal relationships that could have appeared to influence the work reported in this paper.

Acknowledgements

The authors are grateful to the researchers of CREA-VE of Conegliano (TV) and the Laimburg Research Centre (BZ) for providing the grapevine bunches.

Appendix A. Supplementary data

Supplementary data to this article can be found online at https://doi.org/10.1016/j.biosystemseng.2023.10.019.

References

Artem, V., Antoce, A. O., Nmoloanu, I., Ranca, A., & Petrescu, A. (2014). Evaluation of the suistainability of several cultivars for organic growing in the viticultural center of murfatlar. *Horticolture Journal, 58*(10), 119–124. Retrieved from http://horticulturejournal.usamv.ro/pdf/2014/art20.pdf.

Bem, B. P. de, Bogo, A., Everhart, S., Casa, R. T., Gonçalves, M. J., Filho, J. L. M., & da Cunha, I. C. (2015). Effect of Y-trellis and vertical shoot positioning training systems on downy mildew and botrytis bunch rot of grape in highlands of southern Brazil. *Scientia Horticulturae, 185*, 162–166. https://doi.org/10.1016/J.SCIENTA.2015.01.023

Blank, M., Hofmann, M., & Stoll, M. (2019). Seasonal differences in *Vitis vinifera* L. Cv. Pinot noir fruit and wine quality in relation to climate. *Oeno One, 53*(2), 189–203. https://doi.org/10.20870/OENO-ONE.2019.53.2.2427

Boogaard, F. P., van Henten, E. J., & Kootstra, G. (2023). The added value of 3D point clouds for digital plant phenotyping – a case study on internode length measurements in cucumber. *Biosystems Engineering, 234*, 1–12. https://doi.org/10.1016/j.biosystemseng.2023.08.010

Bribiesca, E. (2008). An easy measure of compactness for 2D and 3D shapes. *Pattern Recognition, 41*(2), 543–554. https://doi.org/10.1016/j.patcog.2007.06.029

Chaurasia, A., & Harel, O. (2012). Using AIC in multiple linear regression framework with multiply imputed data. *Health Services & Outcomes Research Methodology, 12*(2–3), 219. https://doi.org/10.1007/S10742-012-0088-8

Chen, X., Ding, H., Yuan, L. M., Cai, J. R., Chen, X., & Lin, Y. (2018). New approach of simultaneous, multi-perspective imaging for quantitative assessment of the compactness of grape bunches. *Australian Journal of Grape and Wine Research, 24*(4), 413–420. https://doi.org/10.1111/ajgw.12349

Cubero, S., Diago, M. P., Blasco, J., Tardaguila, J., Prats-Montalbán, J. M., Ibáñez, J., & Aleixos, N. (2015). A new method for assessment of bunch compactness using automated image analysis. *Australian Journal of Grape and Wine Research, 21*(1), 101–109. https://doi.org/10.1111/ajgw.12118

Gatti, M., Bernizzoni, F., Civardi, S., & Poni, S. (2012). Effects of cluster thinning and preflowering leaf removal on growth and grape composition in cv. Sangiovese. *American Journal of Enology and Viticulture, 63*(3), 325–332. https://doi.org/10.5344/AJEV.2012.11118

Hed, B., Ngugi, H. K., & Travis, J. W. (2009). Relationship between cluster compactness and bunch rot in Vignoles grapes. *Plant Disease, 93*(11), 1195–1201. https://doi.org/10.1094/PDIS-93-11-1195

Herrero-Huerta, M., González-Aguilera, D., Rodriguez-Gonzalvez, P., & Hernández-López, D. (2015). Vineyard yield estimation by automatic 3D bunch modelling in field conditions. *Computers and Electronics in Agriculture, 110*, 17–26. https://doi.org/10.1016/j.compag.2014.10.003

Herrero-Huerta, M., Tardy, H., Morcillo, A., & Gonzalez-gonzalez, E. (2022). Grape bunch architecture by low-cost 3D scanner grape bunch architecture by low-cost 3D scanner. In *Frutic 14th international symposium*. Valencia, Spain: June 2022.

Ivorra, E., Sánchez, A. J., Camarasa, J. G., Diago, M. P., & Tardaguila, J. (2015). Assessment of grape cluster yield components based on 3D descriptors using stereo vision. *Food Control, 50*, 273–282. https://doi.org/10.1016/j.foodcont.2014.09.004

Kocsis, M., Csikász-Krizsics, A., Szata, B., Kovács, S., Nagy, Mátai, A., & Jakab, G. (2018). Regulation of cluster compactness and resistance to *Botrytis cinerea* with β-aminobutyric acid treatment in field-grown grapevine. *Vitis - Journal of Grapevine Research, 57*(1), 35–40. https://doi.org/10.5073/vitis.2018.57.35-40

Ky, I., Lorrain, B., Jourdes, M., Pasquier, G., Fermaud, M., Gény, L., Rey, P., Doneche, B., & Teissedre, P. L. (2012). Assessment of grey mould (*Botrytis cinerea*) impact on phenolic and sensory quality of Bordeaux grapes, musts and wines for two consecutive vintages. *Australian Journal of Grape and Wine Research, 18*(2), 215–226. https://doi.org/10.1111/J.1755-0238.2012.00191.X

Lebon, G., Duchêne, E., Brun, O., Magné, C., & Clément, C. (2004). Flower abscission and inflorescence carbohydrates in sensitive and non-sensitive cultivars of grapevine. *Sexual Plant Reproduction, 17*(2), 71–79. https://doi.org/10.1007/s00497-004-0217-9

Leroux, C., & Tisseyre, B. (2019). How to measure and report within-field variability: A review of common indicators and their sensitivity. *Precision Agriculture, 20*(3), 562–590. https://doi.org/10.1007/s11119-018-9598-x

Li, W., Goodchild, M. F., & Church, R. (2013). An efficient measure of compactness for two-dimensional shapes and its application in regionalization problems. *International Journal of Geographical Information Science, 27*(6), 1227–1250. https://doi.org/10.1080/13658816.2012.752093

Lopes, C. M., & Cadima, J. (2021). Grapevine bunch weight estimation using image-based features: Comparing the predictive performance of number of visible berries and bunch area. *OENO One, 55*(4), 209–226. https://doi.org/10.20870/oeno-one.2021.55.4.4741

Marchal, R., Salmon, T., Gonzalez, R., Kemp, B., Vrigneau, C., Williams, P., & Doco, T. (2020). Impact of *botrytis cinerea* contamination on the characteristics and foamability of yeast macromolecules released during the alcoholic fermentation of a model grape juice. *Molecules, 25*(3), 472. https://doi.org/10.3390/molecules25030472

Marinello, F., Bariani, P., Carmignato, S., & Savio, E. (2009). Geometrical modelling of scanning probe microscopes and characterization of errors. *Measurement Science and Technology, 20*(8), Article 84013. https://doi.org/10.1088/0957-0233/20/8/084013

Marinello, F., Pezzuolo, A., Cillis, D., & Sartori, L. (2016). Kinect 3D reconstruction for quantification of grape bunches volume and mass. In *Proceeding of the 15th international scientific conference in engineering for rural development* (Vols. 25–27, pp. 876–881). Latvia: 05.2016 Jelgava.

Matthews, N. A. (2008). *Aerial and close-range photogrammetric technology: Providing resource documentation, interpretation, and preservation* (p. 3). Denver, Colorado, U.S: U.S. Department of the Interior, Bureau of Land Management, National Operations Center.

Molitor, D., Baus, O., Hoffmann, L., & Beyer, M. (2016). Meteorological conditions determine the thermal-temporal position of the annual botrytis bunch rot epidemic on *Vitis vinifera* L. cv. Riesling grapes. *OENO One, 50*(4), 231–244. https://doi.org/10.20870/oeno-one.2016.50.4.36

Moreau, N., Gentil, C., & Moreau, N. (2014). Study and comparison of surface roughness measurements. March 2014. In *Journees du groupe de Travail en modelisation geometrique* (pp. 1–9). Lyon, France https://hal.science/hal-01068988/document.

Organisation Internationale de la Vigne et du Vin (OIV). (2009). *Of the OIV descriptor list for grape varieties and vitis species* (2nd ed.) (Paris, France).

Palacios, F., Diago, M. P., & Tardaguila, J. (2019). A non-invasive method based on computer vision for grapevine cluster compactness assessment using a mobile sensing platform under field conditions. *Sensors, 19*(17), 3799. https://doi.org/10.3390/s19173799

Palliotti, A., Gatti, M., & Poni, S. (2011). Early leaf removal to improve vineyard efficiency: Gas exchange, source-to-sink balance, and reserve storage responses. *American Journal of Enology and Viticulture, 62*(2), 219–228. https://doi.org/10.5344/ajev.2011.10094

Parliament, E. (2009). *Directive 2009/120/EC of the European Parliament and of the council of 21 October 2009 establishing a framework for community action to achieve the sustainable use of pesticides*.

Poni, S., Casalini, L., Bernizzoni, F., Civardi, S., & Intrieri, C. (2006). Effects of early defoliation on shoot photosynthesis, yield components, and grape composition. *American Journal of Enology and Viticulture, 57*(4), 397–407. https://doi.org/10.5344/ajev.2006.57.4.397

Rapado-Rincón, D., van Henten, E. J., & Kootstra, G. (2023). Development and evaluation of automated localisation and reconstruction of all fruits on tomato plants in a greenhouse based on multi-view perception and 3D multi-object tracking. *Biosystems Engineering, 231*, 78–91. https://doi.org/10.1016/j.biosystemseng.2023.06.003

Ravaz, M. L. (1911). L'effeuillage de la vigne. *Annales de l'Ecole Nationale d'Agriculture de Montpellier, 11*, 216–244.

Rist, F., Gabriel, D., Mack, J., Steinhage, V., Töpfer, R., & Herzog, K. (2019). Combination of an automated 3D field phenotyping workflow and predictive modelling for high-throughput and non-invasive phenotyping of grape bunches. *Remote Sensing, 11*(24), 1–22. https://doi.org/10.3390/rs11242953

Rist, F., Herzog, K., Mack, J., Richter, R., Steinhage, V., & Töpfer, R. (2018). High-precision phenotyping of grape bunch architecture using fast 3d sensor and automation. *Sensors, 18*(3), 763. https://doi.org/10.3390/s18030763

Rose, J. C., Kicherer, A., Wieland, M., Klingbeil, L., Töpfer, R., & Kuhlmann, H. (2016). Towards automated large-scale 3D phenotyping of vineyards under field conditions. *Sensors, 16*(12), 2136. https://doi.org/10.3390/S16122136

Schneider, T., Paulus, G., & Anders, K. H. (2020). Towards predicting vine yield: Conceptualization of 3d grape models and derivation of reliable physical and morphological parameters. *GI_Forum, 8*(1), 73–88. https://doi.org/10.1553/giscience2020_01_s73, 2020.

Stummer, B. E., Francis, I. L., Markides, A. J., & Scott, E. S. (2003). The effect of powdery mildew infection of grape berries on juice and wine composition and on sensory properties of Chardonnay wines. *Australian Journal of Grape and Wine Research, 9*(1), 28–39. https://doi.org/10.1111/j.1755-0238.2003.tb00229.x

Sturges, H. A. (1926). The choice of a class interval case I. computations involving a single series. *Journal of the American Statistical Association, 21*(153), 65–66. https://www.jstor.org/stable/2965501?origin=JSTOR-pdf.

Subramanian, J., & Simon, R. (2013). Overfitting in prediction models-Is it a problem only in high dimensions? *Contemporary Clinical Trials, 32*(2), 636–641. https://doi.org/10.1016/j.cct.2013.06.011

Tardaguila, J., Blanco, J. A., Poni, S., & Diago, M. P. (2012). Mechanical yield regulation in winegrapes: Comparison of early defoliation and crop thinning. *Australian Journal of Grape and Wine Research, 18*(3), 344–352. https://doi.org/10.1111/J.1755-0238.2012.00197.X

Tello, J., Aguirrezábal, R., Hernáiz, S., Larreina, B., Montemayor, M. I., Vaquero, E., & Ibáñez, J. (2015). Multicultivar and multivariate study of the natural variation for grapevine bunch compactness. *Australian Journal of Grape and Wine Research, 21*(2), 277–289. https://doi.org/10.1111/ajgw.12121

Tello, J., Cubero, S., Blasco, J., Tardaguila, J., Aleixos, N., & Ibáñez, J. (2016). Application of 2D and 3D image technologies to characterise morphological attributes of grapevine clusters. *Journal of the Science of Food and Agriculture, 96*(13), 4575–4583. https://doi.org/10.1002/jsfa.7675

Tello, J., & Ibáñez, J. (2014). Evaluation of indexes for the quantitative and objective estimation of grapevine bunch compactness. *Vitis - Journal of Grapevine Research, 53*(1), 9–16. https://doi.org/10.5073/vitis.2014.53.9-16

Tello, J., & Ibáñez, J. (2018). What do we know about grapevine bunch compactness? A state-of-the-art review. *Australian Journal of Grape and Wine Research, 24*(1), 6–23. https://doi.org/10.1111/ajgw.12310

Terleth, J., & Pedri, U. (2010). *Esperienze e prove sperimentali con differenti cloni di Pinot Nero. Centro di sperimentazione agraria di Laimburg*.

Tomasi, C., & Kanade, T. (1991). *Detection and tracking of point features*. Pittsburgh, Pennsylvania: School of computer science, Carnegie Mellon University.

Torres-Sánchez, J., Mesas-Carrascosa, F. J., Santesteban, L. G., Jiménez-Brenes, F. M., Oneka, O., Villa-llop, A., & López-Granados, F. (2021). Grape cluster detection using uav photogrammetric point clouds as a low-cost tool for yield forecasting in vineyards. *Sensors, 21*(9), 3083. https://doi.org/10.3390/s21093083

Townsend, G. R., & Heuberger, J. W. (1943). Methods for estimating losses caused by diseases in fungicide experiments. *Plant Disease Reporter, 27*, 340–343.

Underhill, A., Hirsch, C., & Clark, M. (2020). Image-based phenotyping identifies quantitative trait loci for cluster compactness in grape. *Journal of the American Society for Horticultural Science, 145*(6), 363–373. https://doi.org/10.21273/jashs04932-20

Van Marrewijk, B. M., Vroegindeweij, B. A., Gené-Mola, J., Mencarelli, A., Hemming, J., Mayer, N., Wenger, M., & Kootstra, G. (2022). Evaluation of a boxwood topiary trimming robot. *Biosystems Engineering, 214*, 11–27. https://doi.org/10.1016/j.biosystemseng.2021.12.001

VanderWeide, J., Gottschalk, C., Schultze, S. R., Nasrollahiazar, E., Poni, S., & Sabbatini, P. (2021). Impacts of pre-bloom leaf removal on wine grape production and quality parameters: A systematic review and meta-analysis. *Frontiers in Plant Science, 11*, 621585. https://doi.org/10.3389/fpls.2020.621585

Würz, D. A., Rufato, L., Bogo, A., Allebrandt, R., Pereira de Bem, B., Marcon Filho, J. L., Brighenti, A. F., & Bonin, B. F. (2020). Effects of leaf removal on grape cluster architecture and control of *Botrytis* bunch rot in Sauvignon Blanc grapevines in Southern Brazil. *Crop Protection, 131*, 105079. https://doi.org/10.1016/j.cropro.2020.105079

Xin, B., Liu, S., & Whitty, M. (2020). Three-dimensional reconstruction of *Vitis vinifera* (L.) cvs Pinot Noir and Merlot grape bunch frameworks using a restricted reconstruction grammar based on the stochastic L-system. *Australian Journal of Grape and Wine Research, 26*(3), 207–219. https://doi.org/10.1111/ajgw.12444

Zhang, D., & Lu, G. (2004). Review of shape representation and description techniques. *Pattern Recognition, 37*(1), 1–19. https://doi.org/10.1016/j.patcog.2003.07.008